Two helices control the dynamic crosstalk between the catalytic domains of LRRK2

Jui-Hung Weng[1*], Phillip C. Aoto[1*], Robin Lorenz[2], Jian Wu[1], Sven H. Schmidt[2], Jascha T. Manschwetus[2], Pallavi Kaila-Sharma[1], Sebastian Mathea[3], Stefan Knapp[3], Friedrich W. Herberg[2], Susan S. Taylor[1,4,a]

[1] Department of Pharmacology, University of California, San Diego, USA

[2] Department of Biochemistry, University of Kassel, Germany

[3] Institute for Pharmaceutical Chemistry, Goethe University Frankfurt, Germany

[4] Department of Chemistry and Biochemistry, University of California, San Diego, USA

[*] Authors contributed equally

[a] corresponding author

Email: staylor@ucsd.edu

Abstract

The two major molecular switches in biology, kinases and GTPases, are both contained in the Parkinson's Disease-related Leucine-rich repeat kinase 2 (LRRK2). Using hydrogen-deuterium exchange mass spectrometry (HDX-MS) and Molecular Dynamics (MD) simulations, we generated a comprehensive dynamic allosteric portrait of the C-terminal domains of LRRK2 ($LRRK2_{RCKW}$). We identified two helices that shield the kinase domain and regulate LRRK2 conformation and function. One docking helix in COR-B (Dk-Helix) tethers the COR-B domain to the αC helix of the kinase domain and faces its Activation Loop, while the C-terminal helix (Ct-Helix) extends from the WD40 domain and interacts with both kinase lobes. The Ct-Helix and the N-terminus of the Dk-Helix create a "cap" that regulates the N-Lobe of the kinase domain. Our analyses reveal allosteric sites for pharmacological intervention and confirm the kinase domain as the central hub for conformational control.

Introduction

Parkinson's Disease (PD), a major neurodegenerative disorder, is characterized by chronic and progressive loss of dopaminergic neurons. Mutations in the *PARK8* gene which codes for the Leucine-Rich Repeat Kinase 2 (LRRK2) are the most common cause for genetically driven PD[1]. LRRK2 is a large multi-domain protein that contains an armadillo repeat motif (ARM), ankyrin repeat (ANK), leucine-rich repeat (LRR), ras-of-complex (ROC) GTPase, C-terminal of ROC (COR), protein kinase, and WD40 domains[2]. While crosstalk between kinases and GTPases, the two most important molecular switches in biology, are well-known features in cellular signaling, LRRK2 is one of the few proteins that contains both catalytic domains in the same polypeptide chain[3]. GTP binding to the ROC domain is thought to regulate kinase activity as well as stability and localization[4,5]. Most of the well-known familial mutations are clustered within the ROC, COR and kinase domains; N1473H and R1441C/G/H in the GTPase domain and Y1699C in COR-B lie at the interface between the ROC and COR domains, while G2019S and I2020T are in the highly conserved DFGψ motif within the kinase domain[6,7]. This information collectively suggests that there is considerable crosstalk between the two catalytic domains of LRRK2, but can we capture this crosstalk?

We had previously shown that the kinase domain of LRRK2 is a highly regulated molecular switch. Its conformation regulates more than just kinase activity and plays a crucial role in the intrinsic regulatory processes that mediate subcellular location and activation of LRRK2[8]. Recent breakthroughs in obtaining structure information, including the *in situ* cryo electron tomography (cryo-ET) analysis of LRRK2 polymers associated with microtubules and

the high resolution cryo electron microscopy (cryo-EM) structure of the catalytic C-terminal domains ($LRRK2_{RCKW}$), have provided invaluable structural templates that enabled us to achieve a mechanistic understanding of LRRK2[9,10]. Most recently the cryo-EM structure of full length LRRK2 was also solved at high resolution[11].

Here, we combined hydrogen-deuterium exchange mass spectrometry (HDX-MS) and Gaussian Accelerated Molecular Dynamics (GaMD) simulations to gain insight into the dynamic features of $LRRK2_{RCKW}$, a construct that includes both the kinase and GTPase domains. To build a comprehensive allosteric and dynamic portrait of $LRRK2_{RCKW}$, we first mapped our HDX-MS data onto the $LRRK2_{RCKW}$ cryo-EM structure which gave us a portrait of the solvent accessibility of each peptide. We also assessed the effect of the type I kinase inhibitor MLi-2 and finally used GaMD simulations to monitor the dynamics of $LRRK2_{RCKW}$.

The intrinsic dynamic features of $LRRK2_{RCKW}$ revealed by HDX-MS and GaMD simulations show how the kinase domain is allosterically regulated by its flanking domains. These two techniques allow us to explore the molecular features of domain:domain interfaces and loop dynamics. In this way we identified two distinct motifs that control the kinase domain. These two motifs, the COR-B docking helix (referred to as the Dk-Helix) and the C-terminal helix (Ct-Helix), both impact the overall breathing dynamics of $LRRK2_{RCKW}$. In addition, we showed how the Activation Segment (AS) of the kinase domain faces the ROC:COR-B interface. This interface is unleashed by several PD mutations that cluster in the kinase domain and at the interface between COR-B and the ROC domain. The AS is disordered in the $LRRK2_{RCKW}$ cryo-EM structure, and GaMD simulations allowed us to explore this space. In this inactive conformation, the Dk-

71 Helix is stably anchored onto the αC helix in the N-lobe of the kinase domain, which locks the
72 αC helix into an inactive conformation.

73

74 # Results

75 **Global dynamic portrait of LRRK2$_{RCKW}$ is revealed by HDX-MS and GaMD simulations**

76 To identify the solvent exposed regions of LRRK2$_{RCKW}$, we mapped the HDX-MS data
77 onto the cryo-EM structure of LRRK2$_{RCKW}$[10] (Fig 1a). Our overall HDX-MS coverage of
78 LRRK2$_{RCKW}$, which was >98% (S1 Fig), shows the relative fractional deuterium uptake of each
79 peptide. We previously mapped the HDX-MS profile onto a model of the kinase domain[12]
80 while here we mapped the HDX-MS exchange pattern onto the entire LRRK2$_{RCKW}$ cryo-EM
81 structure. This allows us to capture the crosstalk between and within the C-terminal domains.
82 As shown in S2a Fig., the C-lobe of the kinase domain around the Activation Loop (A-Loop), a
83 part of the surface region of the ROC domain, and parts the COR-B domain show the highest
84 deuterium uptake. These regions are either highly flexible or likely to be unfolded, and some
85 are not resolved in the static cryo-EM structure[10]. In contrast, the core of the ROC domain
86 and the core of the COR-B domain show low deuterium uptake suggesting that they are well-
87 folded and form rigid domains S2b Fig. The WD40 domain, except for several loops, also has
88 less deuterium uptake, which indicates that its core is less dynamic in solution.

89 **Fig 1**. **The overall dynamic of LRRK2$_{RCKW}$.** (a) The relative deuterium uptake after 2 min deuterium
90 exposure is color-coded mapped on the LRRK2$_{RCKW}$ model. Grey color indicates no deuterium uptake

information. The surface of the kinase domain is shown in gray. The highly protected Dk-Helix and the Ct-Helix located at the back of the kinase domain are labelled. (b) Snapshot of $LRRK2_{RCKW}$ in the MD simulation. The surface of each domain is shown in different colors. Left represents the compact architecture of $LRRK2_{RCKW}$. The middle is the structure from cryo-EM. The right represents one of the extended states of $LRRK2_{RCKW}$

There are also regions on the surface of each domain that are highly protected from solvent suggesting that these are domain-domain interfaces. The N-lobe of the kinase domain, for example, is relatively well shielded from solvent in contrast to the highly exposed C-lobe S2b (S2b Fig). The two helices of the COR-A domain at the interface contacting the ROC domain are mostly shielded, indicating that the interaction between COR-A and the ROC domain is stable and persistent. One of the ROC domain helices and the adjacent loops of the COR-B domain all have low deuterium uptake, indicating that the ROC:COR-B interface is also shielded from solvent in this inactive conformation. Parts of the kinase domain N-lobe with low deuterium uptake are mostly shielded by the COR-B-Kinase linker and the COR-B domain. Another interface that is well shielded from solvent lies between the kinase and WD40 domain. The beginning of the WD40 domain, the N-terminal end of the αE helix in the kinase domain and the N-terminus of the C-terminal helix, which extends from the WD40 domain, all have very low deuterium uptake suggesting that the WD40 domain interacts persistently with the C-lobe of the kinase in solution (S2b Fig). This also explains why a stable and active isolated kinase domain of LRRK2 has not been expressed yet.

To investigate the dynamic features of $LRRK2_{RCKW}$ and the interactions within its domains, we performed GaMD simulations to recapitulate the behavior of $LRRK2_{RCKW}$ in solution.

To capture a more accurate representative model of $LRRK2_{RCKW}$ breathing dynamics, we applied enhanced sampling to broadly sample the conformational changes that take place during the simulations. Both extended and compact conformations of $LRRK2_{RCKW}$ are captured by the simulations (Fig. 1b), and the kinase domain is at the center of the breathing dynamics of $LRRK2_{RCKW}$. The COR-B domain persistently interacts with the N-lobe of the kinase during the simulation while the WD40 domain interacts stably with the C-lobe of the kinase domain. The COR-A and ROC domains move as a single rigid body and fluctuate between far and near states relative to the C-lobe of the kinase domain. When the kinase domain is in a closed conformation, the ROC domain and the COR-A domain are brought closer to the C-lobe of the kinase domain (Fig. 1b, left) while in an open conformation (Fig 1b, right), the COR-A domain and ROC domain move further away from the C-lobe of the kinase domain thereby creating a more extended conformation. The dynamic features that bring the ROC domain and the C-lobe of the kinase domain into close proximity correlate with the crosstalk between the kinase and GTPase domains. As described below, our GaMD simulations also revealed many interactions that are potentially involved in allosteric crosstalk within LRRK2 as well as how these interactions might be influenced by PD mutations.

Domain interfaces with the kinase domain.

To better understand how the kinase domain is shielded from solvent, we focused on two dominant helices that embrace the N- and C-lobes of the kinase domain (S3 Fig.). One lies in the COR-B domain (residues 1771-1791) and is buttressed up against the αC helix in the N-lobe while the other helix (residues 2500-2527) lies at the C-terminus and is anchored mainly to the C-lobe of the kinase domain. We refer to these as the COR-B docking helix (or Dk-Helix) and the

C-terminal helix (or Ct-Helix), respectively. In contrast to the well-shielded N-lobe, much of the C-lobe is disordered in the cryo-EM $LRRK2_{RCKW}$ structure, which represents an inactive conformation. In the kinase domain, we focus on the extended Activation Segment (AS), which is typically well-ordered in active kinases and poised to interact with substrates and inhibitors[13]. In the $LRRK2_{RCKW}$ structure, the disordered A-Loop at the beginning of the AS faces the Dk-Helix, while the region at the end of the AS faces ROC and COR-A (S3. Fig.).

Capturing crosstalk between the kinase and COR-B domains.

The COR-B domain plays a critical role in coordinating the communication that takes place between the kinase domain and the ROC domain. Based on our HDX-MS results (Fig. 2), the interface between the N-lobe of the kinase domain and the COR-B domain is mostly shielded from solvent. This surface is dominated by a long amphipathic helix, the Dk-Helix, and the αC helix of the kinase domain (Fig. 2). The Dk-Helix can be divided into three segments based on HDX-MS. While the middle region (residues 1777-1788) shows almost no uptake, the N-terminus shows a slow deuterium exchange. In contrast, the C-terminus of the Dk-Helix is more exposed to solvent but also close to both the disordered A-Loop of the kinase domain and to the ROC domain. It has approximately 50% deuterium uptake at 2 min, which is reduced to 35% when the type I LRRK2 kinase inhibitor MLi-2 is bound. The N-terminus of the αC helix in the kinase domain that binds to the Dk-Helix shows an unusual uptake pattern. The uptake increases at a linear rate signifying a slow exchange without reaching a plateau within 2 min, while binding of MLi-2 significantly protects against uptake. Together, HDX-MS shows that the COR-B:kinase domain interface is mostly shielded from solvent and that the Dk-Helix, in particular, is stably anchored to the N-lobe of the kinase while the N-terminus of the Dk-Helix is

dynamic and communicates with both the kinase and ROC domains. To dissect these interactions more rigorously, we carefully analyzed the three segments of the Dk-Helix that face the αC helix in the kinase domain, the disordered AS and the Ct-Helix (Fig. 3a).

Figure 2. The deuterium uptake around the Dk-Helix. (a) The deuterium uptake of selected peptides is plotted and mapped on the $LRRK2_{RCKW}$ structure. The charts are color coded to the corresponding regions shown. The middle of the Dk-Helix has almost no deuterium uptake suggesting that it is shielded from the solvent. Other peptides that are located at the surface and the activation loop all demonstrate high deuterium uptake. Binding of MLi-2 reduces the deuterium uptake of COR-B-Kinase linker, the αC helix, and the A-Loop. The uptake is also reduced in peptides that are located around the N-terminal or C-terminal ends of the Dk-Helix. Peptide 1426 - 1449 in the ROC domain is the only peptide that its uptake increases when binding to MLi-2. (b) The relative deuterium exchange for each peptide detected from the N-terminus to the C-terminus of $LRRK2_{RKCW}$ in apo state the kinase (Black) and MLi-2 bound (red) conditions at 2 min. The arrows indicate the peptides shown in (a)

Figure 3. Characterization of Dk-Helix. (a) The Dk-Helix, the αC helix and Ct-Helix, and the ROC domain that near the C-terminal end of the Dk-Helix are colored based on the relative fractional uptake. (b) All hydrophobic residues of the Dk-Helix are located on the same side and buried in the COR-B domain while the charged residues that are forming multiple salt bridges with the αC helix are located on the other side. (c) The surface electrostatic potential of the Dk-Helix. The positively charged N-terminal end of the Dk-Helix is interacting with the Ct-Helix, while the C-terminal end is negatively charged and interacts with the ROC domain.

The Dk-Helix has charged residues at both its N- and C- termini while the middle part of the Dk-Helix is amphipathic (Fig. 3b). Multiple hydrophobic residues face the core of the COR-B domain making this a very stable interface (Fig. 3c). On the opposite side, multiple charged

residues interact strongly with the αC helix of the kinase domain through electrostatic interactions, locking the αC helix into an "out" and inactive conformation (Fig. 3c). Typically, in an active kinase the basic residue that lies at the beginning of the αC helix (R1915 in LRRK2) interacts with a phosphate on the A-Loop, which is missing in this structure[14,15]. Our hypothesis is that the N-terminus of the αC helix very likely becomes "unleashed" when the kinase is in an active conformation.

The N-terminus of the Dk-Helix interacts with the COR-B-Kinase linker that is more solvent exposed and wraps around the N-lobe of the kinase domain (Fig. 3a). This region serves as a "cap" for the N-Lobe of the kinase domain indicating that the conformation and flexibility in particular of the N-lobe appears to be tightly controlled by the linker. The N-terminus of the Dk-Helix, which contains two basic residues (R1771 and K1772), also approaches the end of the Ct-Helix that follows the WD40 domain (Fig. 4a) and contains the last few residues of LRRK2 that are thought to be crucial for kinase activity[16,17]. In the $LRRK2_{RCKW}$ cryo-EM structure, the terminal three residues (residues 2525-2527) are disordered[10]. In addition, there is a highly flexible loop in the COR-B domain that lies close to the N-lobe of the kinase domain (Fig. 5a). This loop is solvent exposed and also disordered in the $LRRK2_{RCKW}$ structure. Our MD simulations show a dominant interaction of the C-terminal residue, E2527, both the side chain and the α-carboxyl group, with R1771 and K1772 at the beginning of the Dk-Helix (Fig. 4b).

Figure 4. Capturing crosstalk that is mediated by the N-and C-termini of the Dk-Helix (a) The N-terminal end of the Dk-Helix is in close proximity to the C-terminal residues of the Ct-Helix which are undiscernible in the cryo-EM structure. (b) GaMD simulations capture the interactions between the Dk-Helix with the COR-B-Kinase linker and with the C-terminal end of the Ct-Helix (c) In $LRRK2_{RCKW}$, the Dk-

Helix is stably anchored to the αC helix of the kinase N-lobe. Its N-terminal interacts with the Ct-Helix and the N-lobe of the kinase, while its C-terminal is tethered to the ROC domain and is in close proximity to the A-loop. (d) The C-terminus of the Dk-Helix is anchored to the side chain of R1441 in the ROC domain through W1791. (e) The interaction of E1780 and W1791 with the pathogenic mutation sites R1441 and N1437 on the ROC domain could be captured using GaMD simulations.

Figure 5. The dynamic and of Ct-Helix. (a) The Ct-Helix spans across both the N- and the C-lobe of the kinase domain with the C-terminus being located in close proximity to the Dk-Helix and the COR-B loop. The Ct-Helix and the according interaction sites are shown and colored by their relative fractional uptake. (b) Showing the surface electrostatic potential of the Ct-Helix. The Ct-Helix docks on the kinase domain through the side that is positively charged while the other side is negatively charged and involved in interactions with the N-terminal domains (NTDs). (c) The deuterium uptake of selected peptides is plotted and mapped on the LRRK2RCKW structure. The CORB-kinase loop and the loop in COR-B domain both show high deuterium uptake (70% - 90%), indicating that they are solvent exposed. And their uptake is reduced in the presence of MLi-2.

Crosstalk between the COR-B domain, the ROC domain, and the Activation Loop in the C-lobe of the kinase domain.

The C-terminus of the Dk-Helix is close to both the A-Loop of the kinase domain and the ROC domain, and in the inactive conformation that is captured by the cryo-EM structure, the tip of this helix is anchored to the ROC domain by the side chain of R1441 which binds to the backbone carbonyl of W1791 and helps to “cap” the Dk-Helix (Fig. 4c and d). The C-terminus of the Dk-Helix also faces the A-Loop of the kinase domain, which is likewise disordered in the $LRRK2_{RCKW}$ cryo-EM structure (Fig. 3a). We know that this is a critical region because exchange

of R1441 to either C, G or H is one of the well-documented PD mutations that leads to activation of LRRK2[18]. R1441 as well as N1437, another PD mutation at this interface, are also thought to impair the monomer-dimer cycle of LRRK2 and affect GTPase activity[19].

While a single static conformational state is trapped in the cryo-EM structure, GaMD simulations capture additional potential domain:domain crosstalk that can occur in this region. The simulations suggest, for example, that the side chain of R1441 can also interact with E1790, a residue that is anchored to R1915 in the αC helix of the kinase domain (Fig. 3c and 4e). This is the residue that would be predicted to interact with the phosphorylation site (P-site) in the A-Loop when the kinase is in an active conformation[14,15]. The dynamics of the Dk-Helix would likely be significantly influenced by PD mutations of R1441 and N1437, as well as Y1699C, which would all, in principle, uncouple the ROC domain from the COR-B domain, and thus enhance potential interactions with the kinase domain that may facilitate activation of LRRK2. Each of these pathogenic mutations would unleash the COR-B domain by distinct mechanisms, leaving it free to communicate with the A-Loop of the kinase domain. Based on our GaMD simulations, multiple residues, such as Q2022, Y2023, and R2026 in the A loop, can potentially interact with the C-terminus of the Dk-Helix (S4 fig.) once it is unleashed from the ROC domain. These interactions, as discussed later, could be important for stabilizing the A-Loop in an extended conformation, which would obviously affect LRRK2 kinase phosphorylation and activation.

Capturing the crosstalk between the Ct-Helix and the kinase domain.

The structures of LRRK2 reveal a unique helix at the C-terminus that extends from the WD40 domain and spans both N- and C- lobes of the kinase domain. This Ct-Helix is present in the

inactive $LRRK2_{RCKW}$ cryo-EM structure and is also docked onto the kinase domain in the full-length cryo-EM structure which corresponds to an inactive dimer indicating that it is a very stable helix [9,10],[11]. The combined HDX-MS data captures the dynamic features of the interface of the Ct-Helix with the kinase domain (Fig. 5a). The short segment connecting the kinase and the WD40 domain is embedded between the N-terminus of the Ct-Helix and the C-terminus of the αE helix in the kinase domain and all show low deuterium uptake suggesting a stable interaction between the WD40 domain and the C-lobe of the kinase domain that is shielded from solvent. The Ct-Helix also interacts with the β7-β8 loop in the kinase domain, which is larger in LRRK2 when compared to most kinases (Fig. 5a). The αC-β4 loop of the kinase domain, which is an allosteric docking surface for some kinases such as BRAF[20], is almost completely shielded from solvent (S5 Fig.). The Ct-Helix interacts with the kinase domain through both hydrophobic and positively charged residues on one side (Fig. 5b). The mainly negatively charged residues on the other surface could potentially create a binding interface with the N-terminal domains (NTDs) of LRRK2 when it is inhibited. The recently solved cryo-EM structure of full-length LRRK2 revealed how the ANK and LRR domains interact with the Ct-Helix in the inactive state[11]. The charged surface could also be involved in binding or tethering to substrates or activators when the N-terminal non-catalytic domains are “unleashed” from the kinase domain.

The C-terminal portion of the Ct-Helix directly communicates with the COR-B domain and the N-Lobe of the kinase domain.

The last three residues at the end of the Ct-Helix are at the junction between the COR-B domain and the N-lobe of the kinase domain. This region forms a “cap” for the N-lobe of the kinase

domain (Fig. 6a). The two peptides that cover the COR-B-Kinase linker (residue 1840-1861 and residue 1862-1876) have 70% and 75% uptake of deuterium at 2 min, respectively, and both show a noticeable decrease in deuterium uptake upon binding of MLi-2. The loop in the COR-B domain, which interacts with the C-terminal tail (residues 1713-1724) also shows reduced uptake (Fig. 5c). These changes in deuterium uptake in response to MLi-2 binding indicate correlated changes in dynamics that include both the kinase and COR-B domains and highlights the crosstalk between the GTPase and kinase domains. Our GaMD simulations capture some of the potential interactions that could occur in this region (Fig. 4b and 6b). C-terminal residue E2527 and the free C-terminal carboxyl moiety are of particular interest as the simulations show how the last five residues can fluctuate between different structural states and form different interactions with the COR-B domain, the N-lobe of the kinase domain and the linker between the COR-B domain and the kinase domain. Two arginine residues, R1723 and R1725, in the long loop of the COR-B domain that is disordered in the cryo-EM structures, form H-bonds with E2527 (Fig. 6b). Another two positively charged residues, R1771 and K1772, at the N-terminal end of the Dk-Helix could stabilize the C-terminal tail (residue 2522-2527) based on the simulations (Fig. 4b). R1866 on the COR-B-Kinase linker can also bind to E2527. Other residues, such as E1899 in the loop that connects the β2 and β3 strands of the kinase domain, can also interact with R2523 (Fig. 6b). In addition, the two hydroxyl groups from T2524 and S2525 are also capable of forming H-bonds with either the COR-B or the COR-B-Kinase linker. These interactions that appear in different states during the simulations, show how the C-terminal tail can potentially bridge to the COR-B domain and the kinase domain and thereby contribute to the crosstalk between the kinase and GTPase domains.

Figure 6. Capping of the N-lobe of the kinase. (a) In the LRRK2RCKW cryo-EM structure, the linker from COR-B to the kinase domain lies over the N-Lobe of the kinase domain. Nearby is a disordered loop from COR-B and the disordered three terminal residues. The loops, Dk-Helix and the Ct-Helix are colored based on the relative fractional uptake (b) MD simulations capture potential cross talk between the C-terminal residues, the COR-B-kinase Loop, and basic residues at the N-terminus of the Dk-Helix.

T2524 near the N-terminus is a known auto-phosphorylation site that can be recognized by 14-3-3 binding proteins[21,22]. GaMD simulations with phosphorylated T2524 (pT2524) suggest several new interactions, for example with R1771 and R1886, when the C-terminal tail is closer to the COR-B-Kinase linker (Fig. 6a). When the C-terminal tail is more distant from the N-lobe of the kinase, pT2524 binds to K1772 and R1723 (S6b Fig.). The different networks that can be mediated upon phosphorylation can clearly affect the breathing dynamics of LRRK2 and could in turn affect LRRK2 activity. Also, yet to be resolved is whether 14-3-3 binding would stabilize an active or an inactive dimer.

Capturing the dynamics of the Activation Loop

As a frame of reference for the LRRK2 AS we show the AS of the cAMP-dependent protein kinase (PKA) when the A-Loop is phosphorylated and the kinase is in a fully closed conformation (Fig. 7a). In PKA the AS begins with the DFGψ motif and ends with the APE motif, two of the most highly conserved motifs in the protein kinase superfamily[23]. In between these two motifs are the A-Loop and the P+1 Loop. The APE-αF linker that follows the AS, which typically play an important role in docking of substrates and other proteins[13], and should be considered an extended part of the AS. Our HDX-MS results show that the A-Loop and part of the P+1 Loop in the LRRK2 kinase domain are highly dynamic and likely unfolded (Fig. 2 and S1

movie), which is consistent with the fact that the A-Loop and most of the AS are not resolved in the $LRRK2_{RCKW}$ cryo-EM structure (Fig. 7b). The region extending from the APE motif through to the αF helix is, however, folded, and overlays well with the corresponding region of PKA. Several key residues in this region face out towards the solvent, with the corresponding residues in PKA serving as a docking site for the regulatory subunits (R) (S7 Fig.). Y2050 is also highly conserved in most kinases and it bridges to the backbone residues of this P-site residue when the active kinase is phosphorylated on its A-Loop[24,25] (S8 Fig.). In the cryo-EM structure of LRRK2, this Tyr is not in an active-like conformation. Another interaction in this region is a critical feature that distinguishes the eukaryotic protein kinases (EPKs) from the eukaryotic-like kinases (ELKs), which are their evolutionary precursors[24]. In the ELKs, the A-Loops are short and not dynamic. In addition, the helical domain consisting of the αG, αH, and αI helices is unique to the EPKs. Within this helical domain is a highly conserved Arg between the αH and the αI helices. The A-Loop is anchored to this helical domain by a key and highly conserved electrostatic interaction between E2042 in the APE motif of LRRK and R2122 in the αH-αI loop. In the $LRRK2_{RCKW}$ cryo-EM structure these two residues are close but not within hydrogen bonding distance; however, the interaction between E2042 and R2122 is captured frequently in the GaMD simulations (S9 Fig.).

Figure 7. Comparison of Activation Segments of PKA and LRRK2. (a) The motifs that are embedded in the AS of active PKA are summarized (PDB: 1ATP). The AS begins with the DFG motif and ends with the APE motif, two of the most highly conserved motifs in the protein kinase superfamily. In between these two motifs are the A-Loop and the P+1 Loop. (b) The AS in the inactive LRRK2RCKW structure is mostly disordered. (c) The AS in the inactive full-length LRRK2 is mostly ordered, only residue 2028-2030 are

missing. The A-Loop phosphate in PKA, pT197, is a red sphere and the corresponding residue in LRRK2 is also a red sphere. Additional P-sites in LRRK2 are shown as black spheres.

Surprisingly, when looking at the inactive cryo-EM structure of full-length LRRK2, which also contains ATP, the AS is mostly ordered except for 3 residues (Fig. 7c). In this structure the P+1 loop is ordered in a way that overlays well with PKA. However, the DFGψ motif region is ordered in a helix that is buttressed up against the N-lobe in contrast to an active conformation where the DFGψ motif would be fused to a beta strand that binds to the C-lobe (S8 Fig.). Based on PKA, there are at least two docking motifs embedded within the AS. One docking site is created by the outward facing surface of the A-Loop; the other is created by the outward docking surface of the APE-αF motif. In PKA these two sites are integrated to create a highly dynamic allosteric site that is destroyed by the binding of cAMP (S7 Fig.). In LRRK2, based on our HDX-MS we predict that the A-Loop will reach over to the Dk-Helix while the APE-αF linker will dock onto COR-A. Both states are captured in our GaMD simulations (S10. Fig).

Discussion

The mechanisms that control the intrinsic regulation of LRRK2 include kinase activity as well as targeting to different subcellular sites and the transition between monomeric and dimeric states. In an attempt to capture some of the inter-domain crosstalk, we analyzed the cryo-EM $LRRK2_{RCKW}$ structure[10]. This structure, which represents a static snapshot, was used as our starting point. With HDX-MS and GaMD simulations we were able to explore more deeply in domain:domain interfaces and loop dynamics which allowed us to create a dynamic portrait of $LRRK2_{RCKW}$. Based on the solvent-shielded and solvent-exposed regions, we defined

three rigid bodies, and were able to confirm this domain organization using GaMD simulations (S11 Fig.). The kinase domain is solidly anchored to the WD40 domain as well as the Ct-Helix that extends from the WD40 domain. This explains why it has not been possible to create a stable isolated kinase domain for LRRK2. The catalytically inert COR domain is comprised of two subdomains, referred to as the COR-A and COR-B domains, joined by a flexible linker. The COR-A domain is firmly anchored to the ROC domain so that these two subdomains also move as a rigid body while the COR-B domain functions as a separate rigid body that communicates with both the kinase domain and the ROC domain as well as with the C-terminus (residues 2525-2527). As predicted by Watanabe et al., this highly dynamic COR-B domain is the major mediator of crosstalk between the kinase domain and the ROC domain in the active dimer[9].

GaMD show that domain motions are also embedded within the kinase domain. The kinase domain, for example, toggles between active and inactive states that correlate with opening and closing of the catalytic cleft (Fig. 8 and S12 Fig.). MLi-2, a type I kinase inhibitor, locks the kinase domain into a closed and active-like conformation while a type II inhibitor is hypothesized to lock the kinase domain into an open conformation[10]. The structure of monomeric $LRRK2_{RCKW}$ serves as a model for the inactive kinase while the full-length I2020T LRRK2 mutant docked onto microtubules in a helical manner represents an active dimer[9]. Opening and closing of the kinase cleft, where the N- and C-lobes move as rigid bodies, is determined by the flexibility of the N-Lobe and its ability to communicate with the C-lobe. In its inactive state, it is locked into an open conformation by the two flanking helices, the Dk-Helix in COR-B domain and the Ct-Helix as well as by an unusual DFGψ motif in LRRK2, where the highly conserved Phe is replaced with Tyr (DYGψ)[8]. PD mutations that lead to activation obviously

alter the equilibrium between the active and inactive states. We showed previously how the two PD mutations in the kinase domain (G2019S and I2020T) unleash the inhibitory NTDs, and with our HDX-MS analysis of the kinase domain we showed how the disordered region surrounding the AS becomes more ordered by the binding of MLi-2[12].

In addition to mediating crosstalk between the kinase domain and the GTPase (ROC) domain, the COR-B domain also controls dimerization of the active kinase [9,11]. Embedded within COR-B are two domain:domain interfaces (Fig. 8). The Dk-Helix interface communicates directly with the αC helix in the kinase domain while the COR-B:ROC interface is sensitive to the conformation of the ROC domain as well as PD-related mutations. We hypothesize that these mutations (R1441 and N1437 in the ROC domain and Y1699 in COR-B domain) also unleash the inhibitory NTDs by destabilizing this COR-B:ROC interface[8,26]. One final mutation at this interface (R1398H/K) is actually a protective mutation in both PD and Inflammatory Bowel Disease (IBD)[27]. A final feature of the $LRRK2_{RCKW}$ cryo-EM structure is a bound GDP and T1343 is phosphorylated[26]. Whether this is physiologically important remains to be established; however, T1343 is homologues G12 in RAS and is common disease mutation[28,29].

Figure 8. The interfaces in compact or extend conformation of $LRRK2_{RCKW}$. (a) The Dk-Helix and Ct-Helix are highlighted on the cryo-EM structure of LRRK2RCKW. The pathogenic mutations N1437, R1441 and Y1699 are shown as red spheres. The lines show the domain: domain interfaces: COR-A domain:C-lobe (blue); ROC domain:COR-B domain (red); COR-B domain:N-lobe (black). The kinase domain toggles between open and closed conformations that lead to the compact or extended states of LRRK2RCKW. (b) Cartoon representation of the compact and extended states of LRRK2RCKW. The interaction between the COR-B domain and the N-lobe of the kinase domain, and the ROC domain as well as the

398 COR-B domain remain intact when the COR-A domain moves away from the C-lobe of the kinase in the
399 extended conformation.

400 Communication between the kinase and GTPase domains in LRRK2 is mediated primarily
401 by the domain:domain interfaces of the COR-B domain while direct contact between the kinase
402 domain and COR-A is controlled by the hinging motion of the kinase domain (Fig. 8).
403 Dimerization is also mediated by the COR-B domain as predicted by Watanabe et al. and
404 validated by the structure of full-length LRRK2[9,11]. The two clusters of PD mutations highlight
405 the importance of the COR-B:ROC domain interface and the hinging motion of the kinase
406 domain while all of the mutations potentially "unleash" the inhibition that is imposed by the
407 NTDs. The dominant organizing motif in COR-B is the Dk-Helix while the dominant motif in the
408 kinase domain is the DYGψ motif as described previously[12]. With HDX-MS and GaMD we are
409 beginning to achieve a deeper molecular understanding of these critical domain:domain
410 interfaces as well as loop dynamics, which all contribute to the allosteric regulation of LRRK2
411 and are perturbed by mutations that make LRRK2 a risk factor for PD.

412 # Materials and Methods

413 **Hydrogen-deuterium exchange mass spectrometry**

414 $LRRK2_{RCKW}$ proteins were expressed and purified from Sf9 cell[12]. Hydrogen/deuterium
415 exchange mass spectrometry (HDX-MS) was performed using a Waters Synapt G2Si equipped
416 with nanoACQUITY UPLC system with H/DX technology and a LEAP autosampler. The $LRRK2_{RCKW}$
417 concentration was 5 µM in LRRK2 buffer containing: 20 mM HEPES/NaOH pH 7.4, 800 mM NaCl,
418 0.5 mM TCEP, 5% Glycerol, 2.5 mM $MgCl_2$ and 20 µM GDP. The deuterium uptake was

measured in LRRK2 buffer in the presence and absence of the kinase inhibitor MLi-2 (50 µM). For each deuteration time, 4 µL complex was equilibrated to 25 °C for 5 min and then mixed with 56 µL D_2O LRRK2 buffer for 0, 0.5, 1 or 2 min. The exchange was quenched with an equal volume of quench solution (3 M guanidine, 0.1% formic acid, pH 2.66). The quenched sample (50 µL) was injected into the sample loop, followed by digestion on an in-line pepsin column (immobilized pepsin, Pierce, Inc.) at 15 °C. The resulting peptides were captured on a BEH C18 Vanguard pre-column, separated by analytical chromatography (Acquity UPLC BEH C18, 1.7 µM, 1.0 X 50 mm, Waters Corporation) using a 7-85% acetonitrile gradient in 0.1% formic acid over 7.5 min, and electrosprayed into the Waters SYNAPT G2Si quadrupole time-of-flight mass spectrometer. The mass spectrometer was set to collect data in the Mobility, ESI+ mode; mass acquisition range of 200–2,000 (m/z); scan time 0.4 s. Continuous lock mass correction was accomplished with infusion of leu-enkephalin (m/z = 556.277) every 30 s (mass accuracy of 1 ppm for calibration standard). For peptide identification, the mass spectrometer was set to collect data in MS^E, ESI+ mode instead.

The peptides were identified from triplicate MS^E analyses of 10 µM $LRRK2_{RCKW}$, and data were analyzed using PLGS 3.0 (Waters Corporation). Peptide masses were identified using a minimum number of 250 ion counts for low energy peptides and 50 ion counts for their fragment ions. The peptides identified in PLGS were then analyzed in DynamX 3.0 (Waters Corporation) using a cut-off score of 6.5, error tolerance of 5 ppm and requiring that the peptide be present in at least 2 of the 3 identification runs. The peptides reported on the coverage maps are those from which data were obtained. The relative deuterium uptake for each peptide was calculated by comparing the centroids of the mass envelopes of the

deuterated samples vs. the undeuterated controls[30]. For all HDX-MS data, at least 2 biological replicates were analyzed each with 3 technical replicates. Data are represented as mean values +/- SEM of 3 technical replicates due to processing software limitations, however the LEAP robot provides highly reproducible data for biological replicates. The deuterium uptake was corrected for back-exchange using a global back exchange correction factor (typically 25%) determined from the average percent exchange measured in disordered termini of various proteins[31]. Deuterium uptake plots were generated in DECA (github.com/komiveslab/DECA) and the data are fitted with an exponential curve for ease of viewing[32].

Gaussian accelerated Molecular Dynamics (GaMD) simulation

The $LRRK2_{RCKW}$ model for simulations were prepared based on the reported $LRRK2_{RCKW}$ structure (PDB: 6VP6) using Modeller to model the missing loops[33]. The Protein Preparation Wizard was used to build missing sidechains and model charge states of ionizable residues at neutral pH. Hydrogens and counter ions were added and the models were solvated in a cubic box of TIP4P-EW water[34] and 150 mM KCl with a 10 Å buffer in AMBER tools D.A. Case, 2016 #731}. AMBER16 was used for energy minimization, heating, and equilibration steps, using the CPU code for minimization and heating and GPU code for equilibration. Parameters from the Bryce AMBER parameter database were used for phosphoserine and phosphothreonine[35]. Systems were minimized by 1000 steps of hydrogen-only minimization, 2000 steps of solvent minimization, 2000 steps of ligand minimization, 2000 steps of side-chain minimization, and 5000 steps of all-atom minimization. Systems were heated from 0 K to 300 K linearly over 200 ps with 2 fs time-steps and 10.0 kcal/mol/Å position restraints on protein. Temperature was maintained by the Langevin thermostat. Constant pressure equilibration with an 8 Å non-

bonded cut-off with particle mesh Ewald was performed with 300 ps of protein and peptide restraints followed by 900 ps of unrestrained equilibration. Gaussian accelerated MD (GaMD) was used on GPU enabled AMBER16 to enhance conformational sampling [36]. GaMD applies a Gaussian distributed boost energy to the potential energy surface to accelerate transitions between meta-stable states while allowing accurate reweighting with cumulant expansion. Both dihedral and total potential acceleration were used simultaneously. Potential statistics were collected for 2 ns followed by 2 ns of GaMD during which boost parameters were updated for each simulation. Each GaMD simulation was equilibrated for 10 ns. For each construct 10 independent replicates of 200 ns of GaMD simulation were run in the NVT ensemble, for an aggregate of 2.0 µs of accelerated MD.

Acknowledgements

This work was supported by Michael J. Fox Foundation Grant 11425 (https://www.michaeljfox.org/) (to S.S.T., and F.W.H.), and Ruth L. Kirschstein National Research Service Award NIH/National Cancer Institute T32 CA009523 (to P.C.A.). JTM was supported by an Otto-Braun Fund Predoctoral Fellowship (B. Braun Melsungen AG). S.M. and S.K. are grateful for support from the Deutsche Forschungsgemeinschaft (DFG) (HE 1818/11) and Structural Genomics Consortium (SGC), a registered charity that receives funds from AbbVie, Bayer Pharma AG, Boehringer Ingelheim, Canada Foundation for Innovation, Eshelman Institute for Innovation, Genome Canada, Innovative Medicines Initiative (875510), Janssen, Merck KGaA Darmstadt Germany, Merck Sharp and Dohme (MSD), Novartis Pharma AG, Ontario Ministry of Economic Development and Innovation. The Synapt G2Si HD/X mass spectrometer was obtained from shared instrumentation NIH Grant S10 OD016234 (to S.S.).

The funders had no role in study design, data collection and analysis, decision to publish, or preparation of the manuscript.

Author Contributions

J.-H.W., P.C.A., S.M., F.W.H., and S.S.T. designed research; J.-H.W., P.C.A., and S.M. performed research; J.-H.W., P.C.A., S.H.S., R.L., J.W., J. T. M., P. K.-S., S.M., S. K., F.W.H., and S.S.T. analyzed data; and J.-H.W., P.C.A., R.L., J.W., J. T. M., P. K.-S., F.W.H., and S.S.T. wrote the paper. All author reviews the manuscript.

Competing Interests statement

The authors have no competing interests.

References

1. Benitez BA, Davis AA, Jin SC, Ibanez L, Ortega-Cubero S, et al. (2016) Resequencing analysis of five Mendelian genes and the top genes from genome-wide association studies in Parkinson's Disease. Mol Neurodegener 11: 29.
2. Mata IF, Wedemeyer WJ, Farrer MJ, Taylor JP, Gallo KA (2006) LRRK2 in Parkinson's disease: protein domains and functional insights. Trends Neurosci 29: 286-293.
3. Tomkins JE, Dihanich S, Beilina A, Ferrari R, Ilacqua N, et al. (2018) Comparative Protein Interaction Network Analysis Identifies Shared and Distinct Functions for the Human ROCO Proteins. Proteomics 18: e1700444.
4. Sheng Z, Zhang S, Bustos D, Kleinheinz T, Le Pichon CE, et al. (2012) Ser1292 autophosphorylation is an indicator of LRRK2 kinase activity and contributes to the cellular effects of PD mutations. Sci Transl Med 4: 164ra161.
5. Nguyen AP, Moore DJ (2017) Understanding the GTPase Activity of LRRK2: Regulation, Function, and Neurotoxicity. Adv Neurobiol 14: 71-88.
6. West AB, Moore DJ, Choi C, Andrabi SA, Li X, et al. (2007) Parkinson's disease-associated mutations in LRRK2 link enhanced GTP-binding and kinase activities to neuronal toxicity. Hum Mol Genet 16: 223-232.
7. Cookson MR (2017) Mechanisms of Mutant LRRK2 Neurodegeneration. Adv Neurobiol 14: 227-239.
8. Schmidt SH, Knape MJ, Boassa D, Mumdey N, Kornev AP, et al. (2019) The dynamic switch mechanism that leads to activation of LRRK2 is embedded in the DFGpsi motif in the kinase domain. Proc Natl Acad Sci U S A.
9. Watanabe R, Buschauer R, Bohning J, Audagnotto M, Lasker K, et al. (2020) The In Situ Structure of Parkinson's Disease-Linked LRRK2. Cell 182: 1508-1518 e1516.
10. Deniston CK, Salogiannis J, Mathea S, Snead DM, Lahiri I, et al. (2020) Structure of LRRK2 in Parkinson's disease and model for microtubule interaction. Nature.
11. Myasnikov A, Zhu H, Hixson P, Xie B, Yu K, et al. (2021) Structural analysis of the full-length human LRRK2. Cell.
12. Schmidt SH, Weng JH, Aoto PC, Boassa D, Mathea S, et al. (2021) Conformation and dynamics of the kinase domain drive subcellular location and activation of LRRK2. Proc Natl Acad Sci U S A 118.
13. Taylor SS, Kornev AP (2011) Protein kinases: evolution of dynamic regulatory proteins. Trends Biochem Sci 36: 65-77.
14. Nolen B, Taylor S, Ghosh G (2004) Regulation of protein kinases; controlling activity through activation segment conformation. Mol Cell 15: 661-675.
15. Johnson LN, Noble ME, Owen DJ (1996) Active and inactive protein kinases: structural basis for regulation. Cell 85: 149-158.
16. Kett LR, Boassa D, Ho CC, Rideout HJ, Hu J, et al. (2012) LRRK2 Parkinson disease mutations enhance its microtubule association. Hum Mol Genet 21: 890-899.
17. Rudenko IN, Kaganovich A, Hauser DN, Beylina A, Chia R, et al. (2012) The G2385R variant of leucine-rich repeat kinase 2 associated with Parkinson's disease is a partial loss-of-function mutation. Biochem J 446: 99-111.
18. Haugarvoll K, Wszolek ZK (2009) Clinical features of LRRK2 parkinsonism. Parkinsonism Relat Disord 15 Suppl 3: S205-208.
19. Huang X, Wu C, Park Y, Long X, Hoang QQ, et al. (2019) The Parkinson's disease-associated mutation N1437H impairs conformational dynamics in the G domain of LRRK2. FASEB J 33: 4814-4823.

539 20. Hu J, Stites EC, Yu H, Germino EA, Meharena HS, et al. (2013) Allosteric activation of functionally
540 asymmetric RAF kinase dimers. Cell 154: 1036-1046.
541 21. Pungaliya PP, Bai Y, Lipinski K, Anand VS, Sen S, et al. (2010) Identification and characterization of a
542 leucine-rich repeat kinase 2 (LRRK2) consensus phosphorylation motif. PLoS One 5: e13672.
543 22. Manschwetus JT, Wallbott M, Fachinger A, Obergruber C, Pautz S, et al. (2020) Binding of the Human
544 14-3-3 Isoforms to Distinct Sites in the Leucine-Rich Repeat Kinase 2. Front Neurosci 14: 302.
545 23. Johnson DA, Akamine P, Radzio-Andzelm E, Madhusudan M, Taylor SS (2001) Dynamics of cAMP-
546 dependent protein kinase. Chem Rev 101: 2243-2270.
547 24. Taylor SS, Keshwani MM, Steichen JM, Kornev AP (2012) Evolution of the eukaryotic protein kinases
548 as dynamic molecular switches. Philos Trans R Soc Lond B Biol Sci 367: 2517-2528.
549 25. Krupa A, Preethi G, Srinivasan N (2004) Structural modes of stabilization of permissive
550 phosphorylation sites in protein kinases: distinct strategies in Ser/Thr and Tyr kinases. J Mol Biol
551 339: 1025-1039.
552 26. Taylor SS, Kaila-Sharma P, Weng JH, Aoto P, Schmidt SH, et al. (2020) Kinase Domain Is a Dynamic
553 Hub for Driving LRRK2 Allostery. Front Mol Neurosci 13: 538219.
554 27. Hui KY, Fernandez-Hernandez H, Hu J, Schaffner A, Pankratz N, et al. (2018) Functional variants in the
555 LRRK2 gene confer shared effects on risk for Crohn's disease and Parkinson's disease. Sci Transl
556 Med 10.
557 28. Deng J, Lewis PA, Greggio E, Sluch E, Beilina A, et al. (2008) Structure of the ROC domain from the
558 Parkinson's disease-associated leucine-rich repeat kinase 2 reveals a dimeric GTPase. Proc Natl
559 Acad Sci U S A 105: 1499-1504.
560 29. Prior IA, Lewis PD, Mattos C (2012) A comprehensive survey of Ras mutations in cancer. Cancer Res
561 72: 2457-2467.
562 30. Wales TE, Fadgen KE, Gerhardt GC, Engen JR (2008) High-speed and high-resolution UPLC separation
563 at zero degrees Celsius. Anal Chem 80: 6815-6820.
564 31. Ramsey KM, Dembinski HE, Chen W, Ricci CG, Komives EA (2017) DNA and IkappaBalpha Both Induce
565 Long-Range Conformational Changes in NFkappaB. J Mol Biol 429: 999-1008.
566 32. Lumpkin RJ, Komives EA (2019) DECA, A Comprehensive, Automatic Post-processing Program for
567 HDX-MS Data. Mol Cell Proteomics 18: 2516-2523.
568 33. Sali A, Blundell TL (1993) Comparative protein modelling by satisfaction of spatial restraints. J Mol
569 Biol 234: 779-815.
570 34. Horn HW, Swope WC, Pitera JW, Madura JD, Dick TJ, et al. (2004) Development of an improved four-
571 site water model for biomolecular simulations: TIP4P-Ew. J Chem Phys 120: 9665-9678.
572 35. Homeyer N, Horn AH, Lanig H, Sticht H (2006) AMBER force-field parameters for phosphorylated
573 amino acids in different protonation states: phosphoserine, phosphothreonine, phosphotyrosine,
574 and phosphohistidine. J Mol Model 12: 281-289.
575 36. Miao Y, Feher VA, McCammon JA (2015) Gaussian Accelerated Molecular Dynamics: Unconstrained
576 Enhanced Sampling and Free Energy Calculation. J Chem Theory Comput 11: 3584-3595.

577

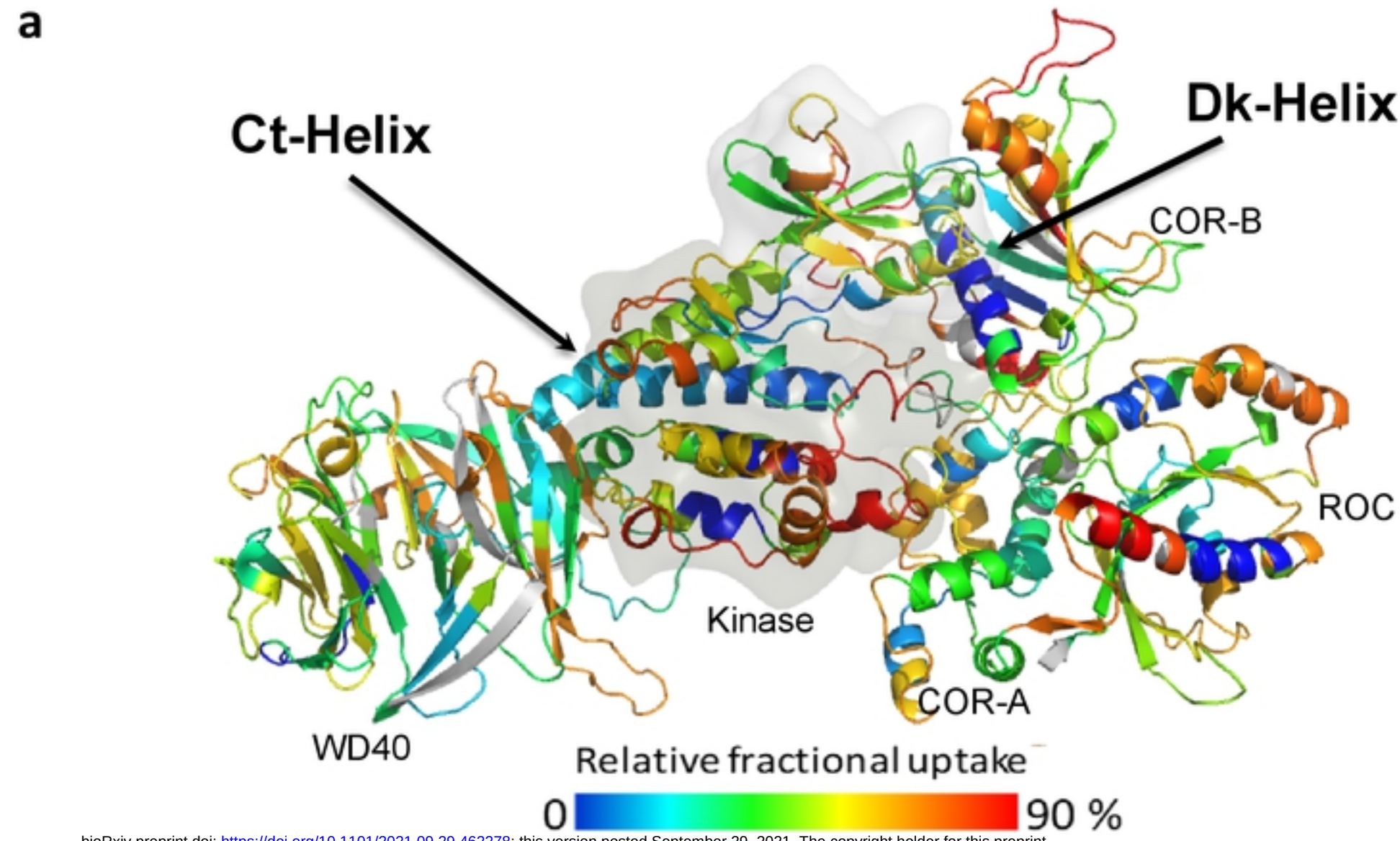

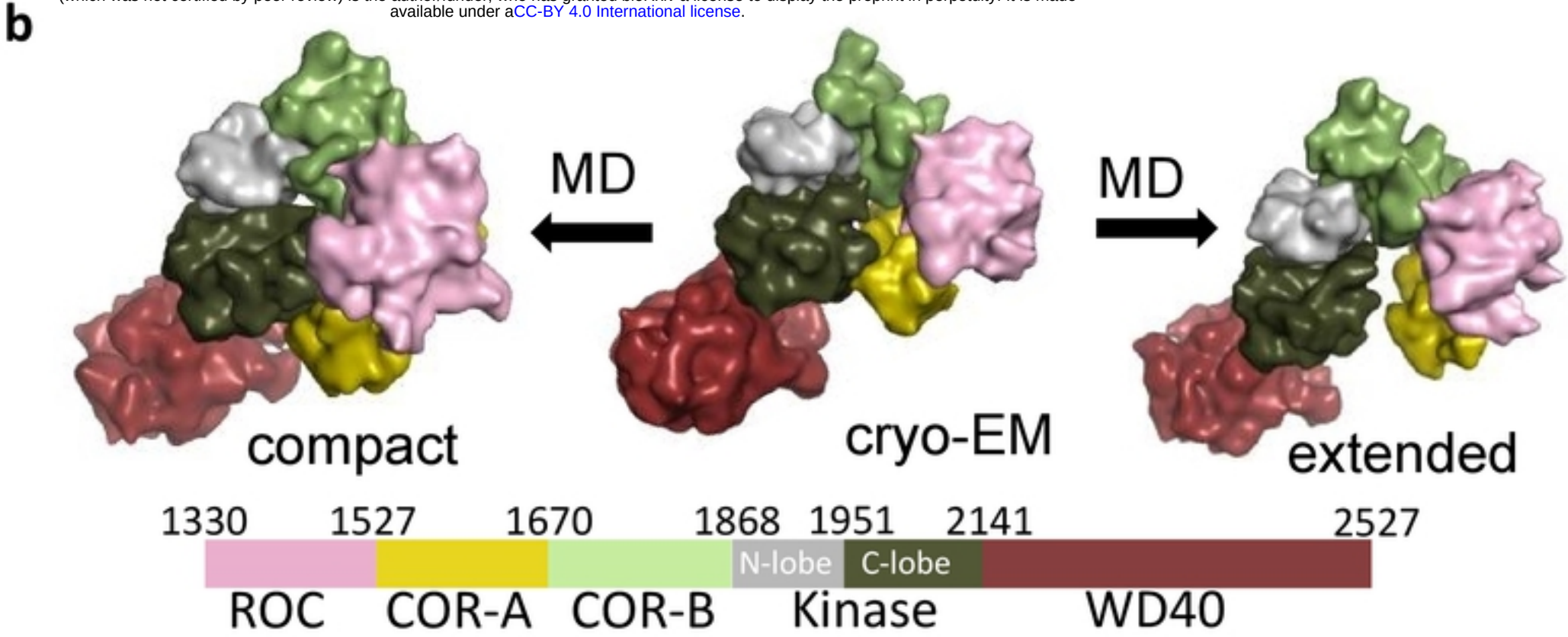

Figure 1. The overall dynamic of LRRK2$_{RCKW}$. (a) The relative deuterium uptake after 2 min deuterium exposure is color-coded mapped on the LRRK2$_{RCKW}$ model. Grey color indicates no deuterium uptake information. The surface of the kinase domain is shown in gray. The highly protected Dk-Helix and the Ct-Helix located at the back of the kinase domain are labelled. (B) Snapshot of LRRK2$_{RCKW}$ in the MD simulation. The surface of each domain is shown in different colors. Left represents the compact architecture of LRRK2$_{RCKW}$. The middle is the structure from cryo-EM. The right represents one of the extended states of LRRK2$_{RCKW}$.

Figure 1

Figure 2. The deuterium uptake around the Dk-Helix. (a) The deuterium uptake of selected peptides is plotted and mapped on the $LRRK2_{RCKW}$ structure. The charts are color coded to the corresponding regions shown. The middle of the Dk-Helix has almost no deuterium uptake suggesting that it is shielded from the solvent. Other peptides that are located at the surface and the activation loop all demonstrate high deuterium uptake. Binding of MLi-2 reduces the deuterium uptake of COR-B-Kinase linker, the αC helix, and the A-Loop. The uptake is also reduced in peptides that are located around the N-terminal or C-terminal ends of the Dk-Helix. Peptide 1426 - 1449 in the ROC domain is the only peptide that its uptake increases when binding to MLi-2. (b) The relative deuterium exchange for each peptide detected from the N-terminus to the C-terminus of $LRRK2_{RKCW}$ in apo state the kinase (Black) and MLi-2 bound (red) conditions at 2 min. The arrows indicate the peptides shown in (a).

Figure 2

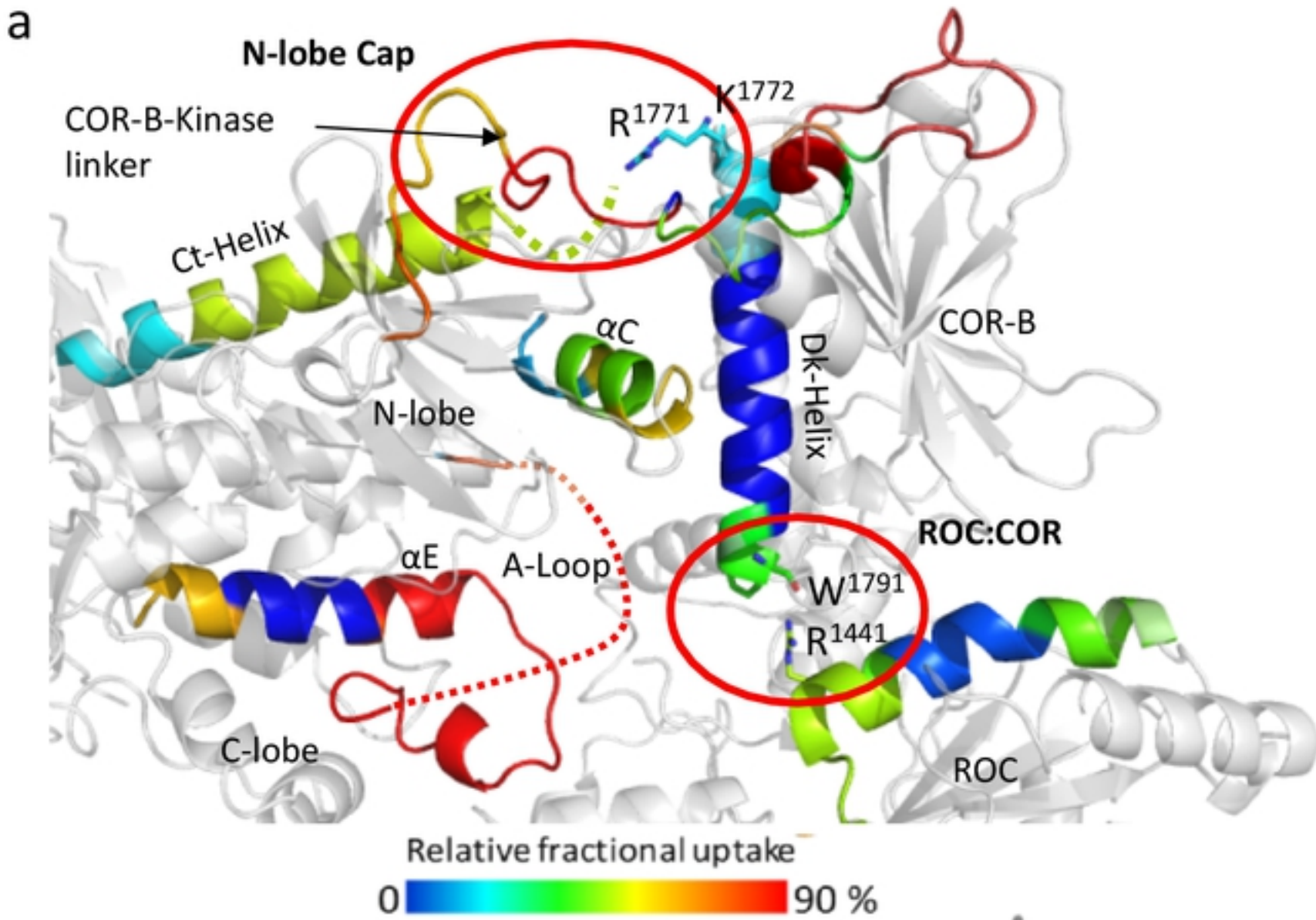

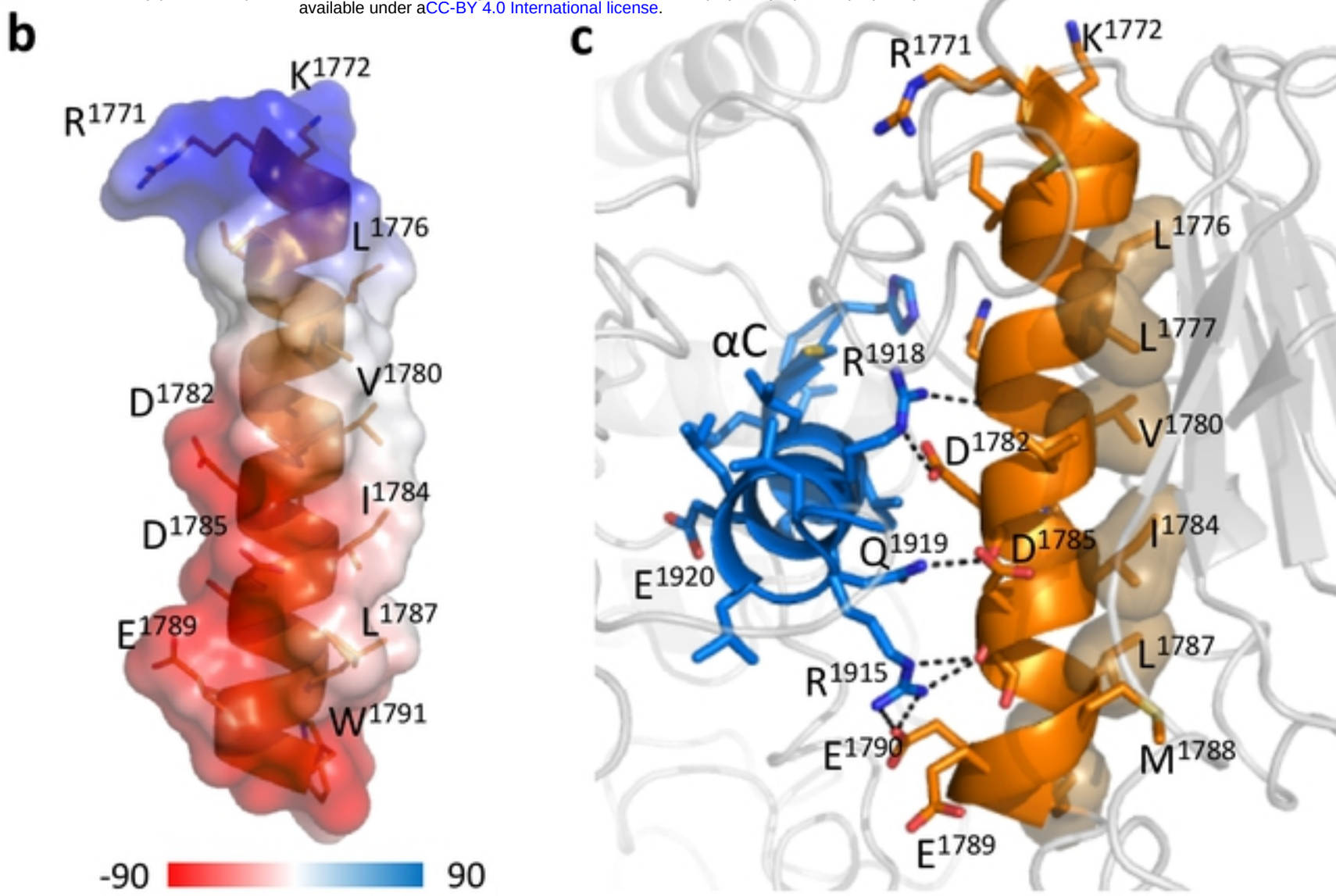

Figure 3. Characterization of Dk-Helix. (a) The Dk-Helix, the αC helix and Ct-Helix, and the ROC domain that near the C-terminal end of the Dk-Helix are colored based on the relative fractional uptake. (b) All hydrophobic residues of the Dk-Helix are located on the same side and buried in the COR-B domain while the charged residues that are forming multiple salt bridges with the αC helix are located on the other side. (c) The surface electrostatic potential of the Dk-Helix. The positively charged N-terminal end of the Dk-Helix is interacting with the Ct-Helix, while the C-terminal end is negatively charged and interacts with the ROC domain.

Figure 3

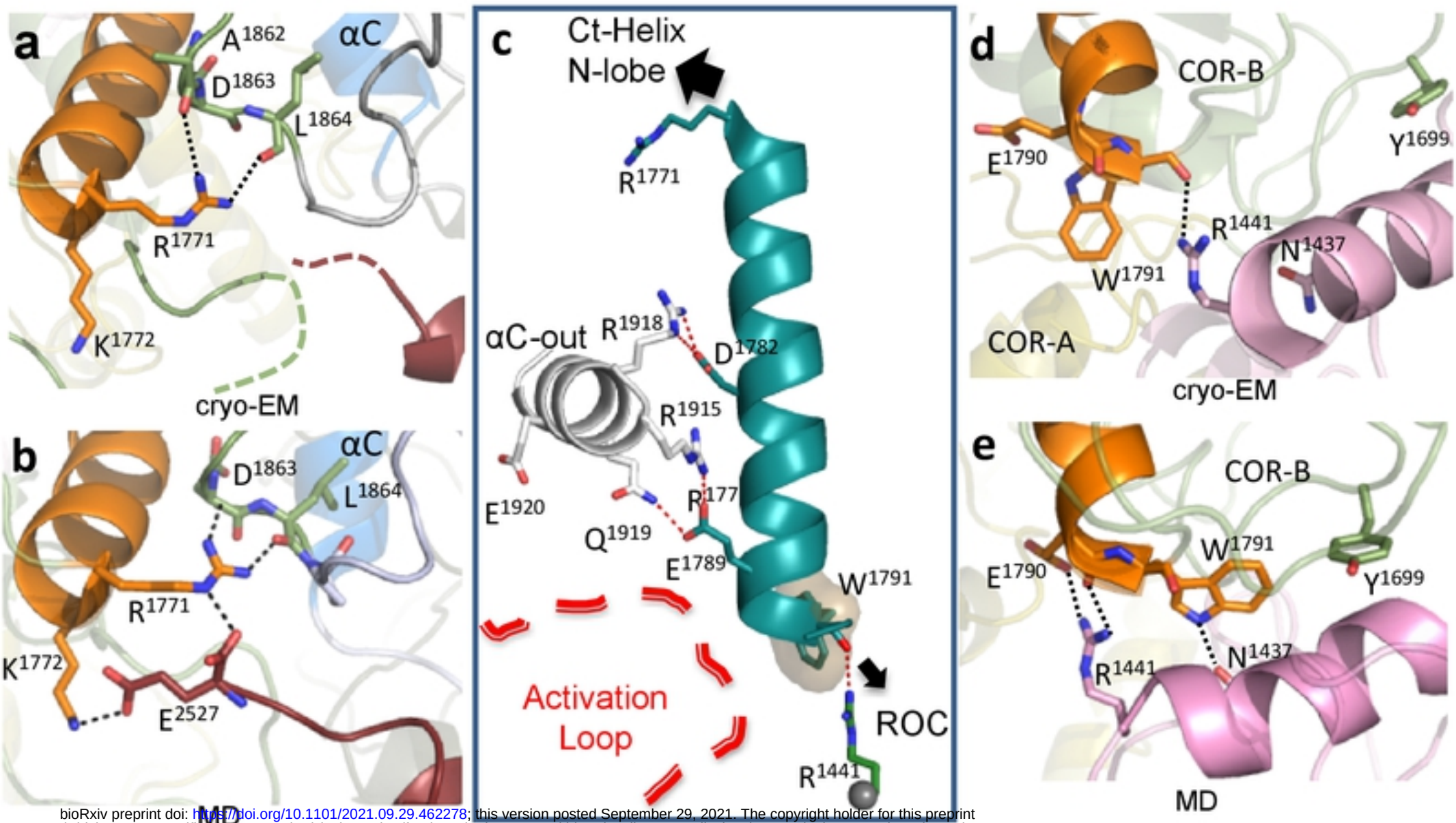

Figure 4. Capturing crosstalk that is mediated by the N-and C-termini of the Dk-Helix (a) The N-terminal end of the Dk-Helix is in close proximity to the C-terminal residues of the Ct-Helix which are undiscernible in the cryo-EM structure. (b) GaMD simulations capture the interactions between the Dk-Helix with the COR-B-Kinase linker and with the C-terminal end of the Ct-Helix (c) In $LRRK2_{RCKW}$, the Dk-Helix is stably anchored to the αC helix of the kinase N-lobe. Its N-terminal interacts with the Ct-Helix and the N-lobe of the kinase, while its C-terminal is tethered to the ROC domain and is in close proximity to the A-loop. (d) The C-terminus of the Dk-Helix is anchored to the side chain of R1441 in the ROC domain through W1791. (e) The interaction of E1780 and W1791 with the pathogenic mutation sites R1441 and N1437 on the ROC domain could be captured using GaMD simulations.

Figure 4

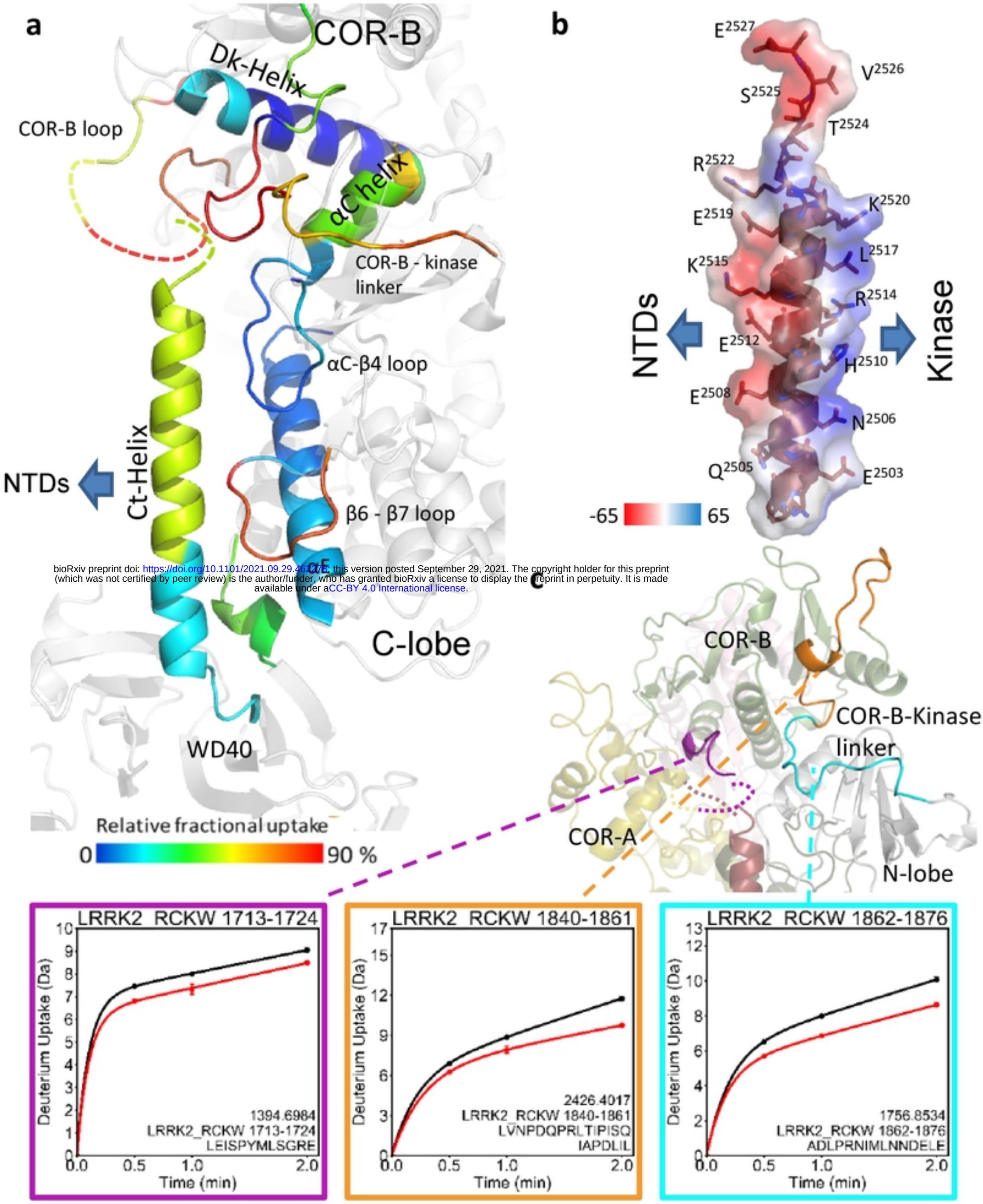

Figure 5. The dynamic and of Ct-Helix. (a) The Ct-Helix spans across both the N- and the C-lobe of the kinase domain with the C-terminus being located in close proximity to the Dk-Helix and the COR-B loop. The Ct-Helix and the according interaction sites are shown and colored by their relative fractional uptake. (b) Showing the surface electrostatic potential of the Ct-Helix. The Ct-Helix docks on the kinase domain through the side that is positively charged while the other side is negatively charged and involved in interactions with the N-terminal domains (NTDs). (c) The deuterium uptake of selected peptides is plotted and mapped on the LRRK2RCKW structure. The CORB-kinase loop and the loop in COR-B domain both show high deuterium uptake (70% - 90%), indicating that they are solvent exposed. And their uptake is reduced in the presence of MLi-2.

Figure 5

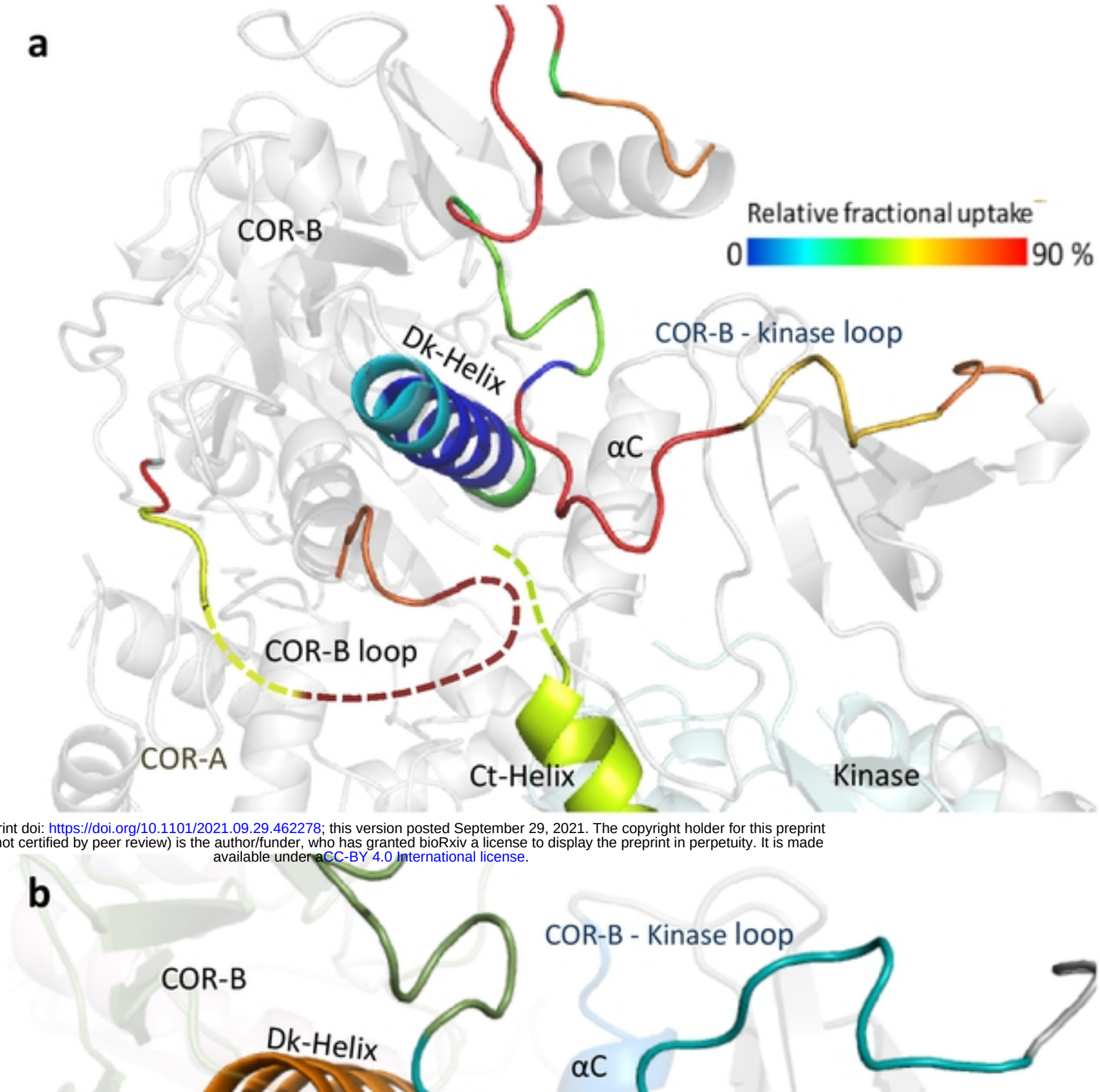

Figure 6. Capping of the N-lobe of the kinase. (a) In the LRRK2RCKW cryo-EM structure, the linker from COR-B to the kinase domain lies over the N-Lobe of the kinase domain. Nearby is a disordered loop from COR-B and the disordered three terminal residues. The loops, Dk-Helix and the Ct-Helix are colored based on the relative fractional uptake (b) MD simulations capture potential cross talk between the C-terminal residues, the COR-B-kinase Loop, and basic residues at the N-terminus of the Dk-Helix.

Figure 6

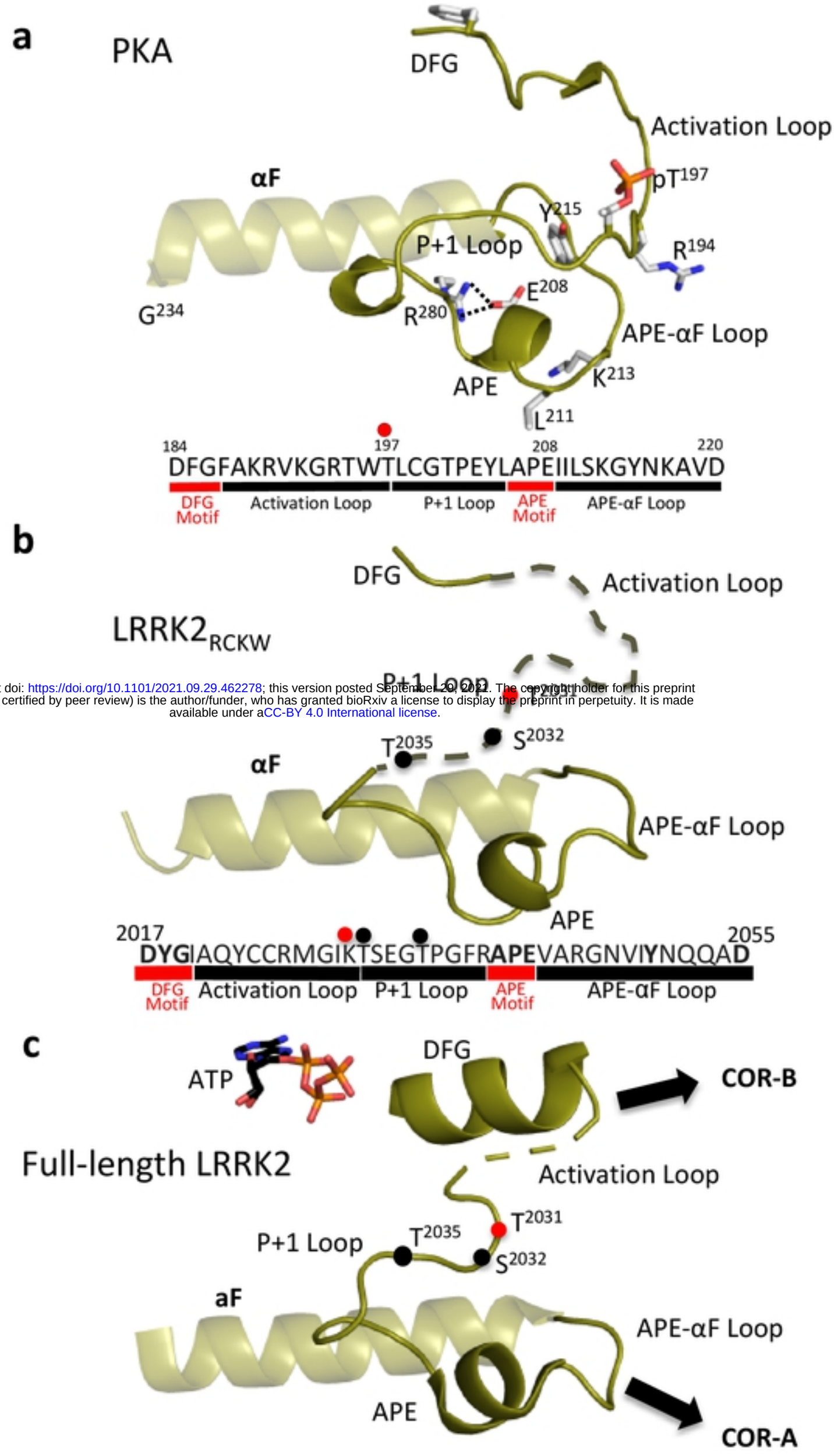

Figure 7. Comparison of Activation Segments of PKA and LRRK2. (a) The motifs that are embedded in the AS of active PKA are summarized (PDB: 1ATP). The AS begins with the DFG motif and ends with the APE motif, two of the most highly conserved motifs in the protein kinase superfamily. In between these two motifs are the A-Loop and the P+1 Loop. (b) The AS in the inactive LRRK2RCKW structure is mostly disordered. (c) The AS in the inactive full-length LRRK2 is mostly ordered, only residue 2028-2030 are missing. The A-Loop phosphate in PKA, pT197, is a red sphere and the corresponding residue in LRRK2 is also a red sphere. Additional P-sites in LRRK2 are shown as black spheres.

Figure 7

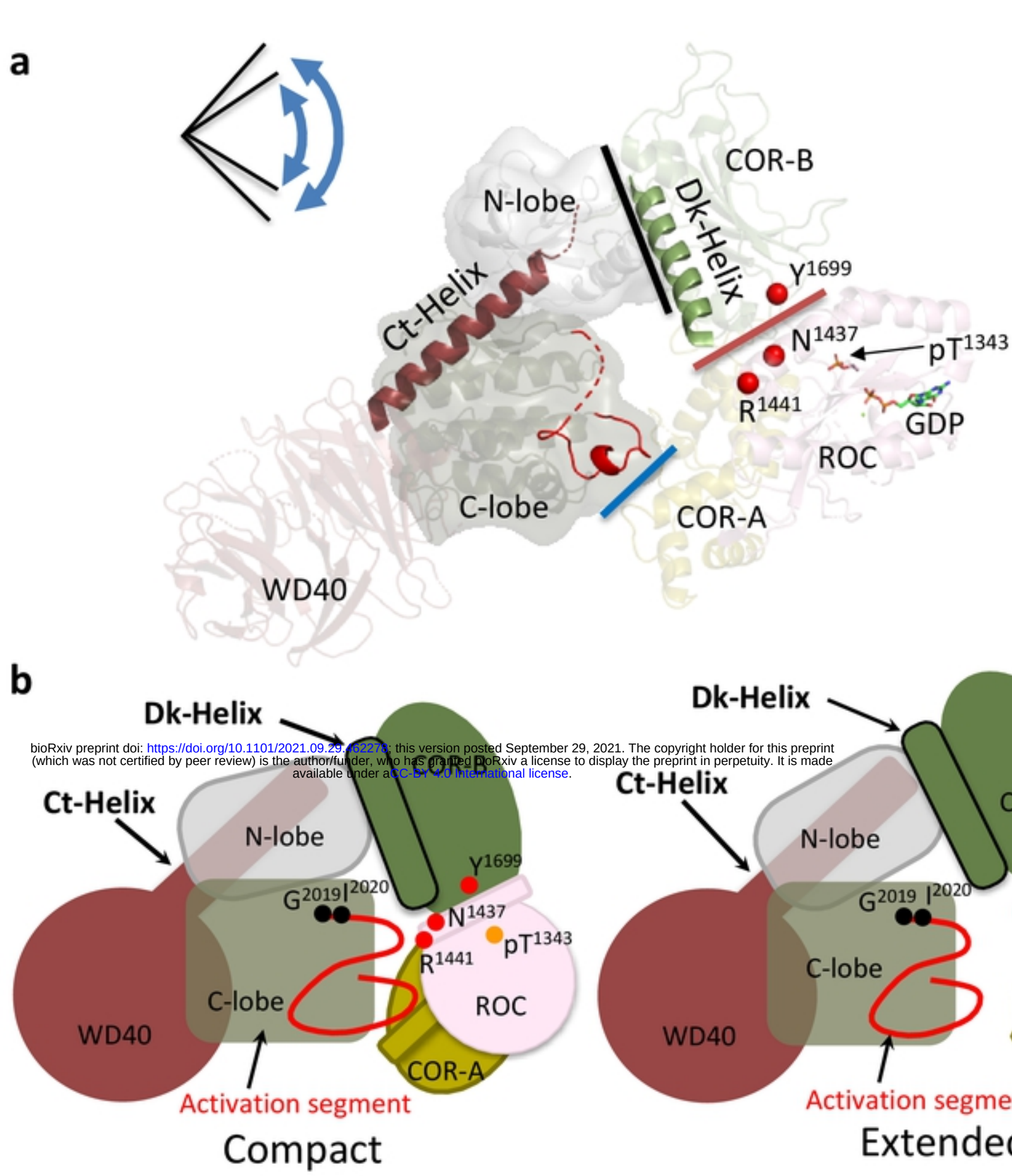

Figure 8. The interfaces in compact or extend conformation of $LRRK2_{RCKW}$. (a) The Dk-Helix and Ct-Helix are highlighted on the cryo-EM structure of LRRK2RCKW. The pathogenic mutations N1437, R1441 and Y1699 are shown as red spheres. The lines show the domain: domain interfaces: COR-A domain:C-lobe (blue); ROC domain:COR-B domain (red); COR-B domain:N-lobe (black). The kinase domain toggles between open and closed conformations that lead to the compact or extended states of LRRK2RCKW. (b) Cartoon representation of the compact and extended states of LRRK2RCKW. The interaction between the COR-B domain and the N-lobe of the kinase domain, and the ROC domain as well as the COR-B domain remain intact when the COR-A domain moves away from the C-lobe of the kinase in the extended conformation.

Figure 8